The Astrophysical Journal Letters, 792:L5 (5pp), 2014 September 1 doi:10.1088/2041-8205/792/1/L5

HIGH D_2O/HDO RATIO IN THE INNER REGIONS OF THE LOW-MASS PROTOSTAR NGC 1333 IRAS2A*

A. Coutens[1,2], J. K. Jørgensen[1,2], M. V. Persson[3], E. F. van Dishoeck[3,4], C. Vastel[5,6], and V. Taquet[7]
[1] Niels Bohr Institute, University of Copenhagen, Juliane Maries Vej 30, DK-2100 Copenhagen Ø, Denmark; acoutens@nbi.dk
[2] Centre for Star and Planet Formation, Natural History Museum of Denmark, University of Copenhagen, Øster Voldgade 5-7, DK-1350 Copenhagen K, Denmark
[3] Leiden Observatory, Leiden University, P.O. Box 9513, 2300 RA Leiden, The Netherlands
[4] Max-Planck-Institut für Extraterrestrische Physik, Giessenbachstrasse 1, D-85748 Garching, Germany
[5] Université de Toulouse, UPS-OMP, IRAP, F-31062 Toulouse, France
[6] CNRS, IRAP, 9 Av. Colonel Roche, BP 44346, F-31028 Toulouse Cedex 4, France
[7] NASA Postdoctoral Program Fellow, NASA Goddard Space Flight Center, 8800 Greenbelt Road, Greenbelt, MD 20770, USA
Received 2014 June 30; accepted 2014 July 24; published 2014 August 11

ABSTRACT

Water plays a crucial role both in the interstellar medium and on Earth. To constrain its formation mechanisms and its evolution through the star formation process, the determination of the water deuterium fractionation ratios is particularly suitable. Previous studies derived HDO/H_2O ratios in the warm inner regions of low-mass protostars. We here report a detection of the D_2O $1_{1,0}$–$1_{0,1}$ transition toward the low-mass protostar NGC 1333 IRAS2A with the Plateau de Bure interferometer: this represents the first interferometric detection of D_2O—and only the second solar-type protostar for which this isotopologue is detected. Using the observations of the HDO $5_{4,2}$–$6_{3,3}$ transition simultaneously detected and three other HDO lines previously observed, we show that the HDO line fluxes are well reproduced with a single excitation temperature of 218 ± 21 K and a source size of ∼0.″5. The D_2O/HDO ratio is $\sim(1.2 \pm 0.5) \times 10^{-2}$, while the use of previous $H_2^{18}O$ observations give an HDO/H_2O ratio of $\sim(1.7 \pm 0.8) \times 10^{-3}$, i.e., a factor of seven lower than the D_2O/HDO ratio. These results contradict the predictions of current grain surface chemical models and indicate that either the surface deuteration processes are poorly understood or that both sublimation of grain mantles and water formation at high temperatures ($\gtrsim$230 K) take place in the inner regions of this source. In the second scenario, the thermal desorption of the grain mantles would explain the high D_2O/HDO ratio, while water formation at high temperature would explain significant extra production of H_2O leading to a decrease of the HDO/H_2O ratio.

Key words: astrochemistry – ISM: individual objects (NGC 1333 IRAS2A) – ISM: molecules – stars: protostars

Online-only material: color figure

1. INTRODUCTION

In addition to being a crucial ingredient for the emergence of life on Earth, water is omnipresent in the interstellar medium and is detected both in the gas and solid phases (e.g., van Dishoeck et al. 2013). Observations of its deuterated forms are necessary to understand how water forms and how it evolves during star formation until its incorporation into comets and asteroids that may then deliver water to planets through impacts (e.g., Raymond et al. 2004; Hartogh et al. 2011). Indeed, the water deuterium fractionation is quite sensitive to the conditions (temperature and density) in which water forms. The relative abundance ratios between H_2O, HDO, and D_2O act then as a tracer of the water formation and alteration (e.g., Ceccarelli et al. 2014). They can be estimated at different stages of the star formation process in order to constrain the water evolution history.

Numerous lines of HDO have been detected toward low-mass protostars with ground-based single-dish telescopes (Stark et al. 2004; Parise et al. 2005; Liu et al. 2011) as well as the Heterodyne Instrument for Far-Infrared (HIFI) on board the *Herschel Space Observatory* (Coutens et al. 2012, 2013b). A few excited lines have also been detected with interferometers (Codella et al. 2010; Persson et al. 2013, 2014; Taquet et al. 2013a), showing that their emission mainly arises from the warm inner regions of low-mass protostars.

Due to its double deuteration, heavy water (D_2O) is more challenging to detect. The para-D_2O $1_{1,0}$–$1_{0,1}$ fundamental transition was, however, detected at 316.8 GHz with the James Clerk Maxwell Telescope toward the Class 0 protostar IRAS 16293−2422 by Butner et al. (2007). Two additional fundamental transitions ($1_{1,1}$–$0_{0,0}$ and $2_{1,2}$–$1_{0,1}$) were detected in absorption toward the same source with the HIFI instrument at 607.3 and 897.9 GHz, respectively (Vastel et al. 2010; Coutens et al. 2013a). These absorption components, also seen for HDO, arise from a cold extended layer surrounding the protostar, where gaseous water is assumed to be produced by photodesorption mechanisms (cosmic-ray induced and/or external UV field). Thanks to one-dimensional (1D) radiative transfer modeling of these three D_2O lines and other HDO and $H_2^{18}O$ lines (Coutens et al. 2012, 2013a), the water deuterium fractionation was found to be extremely high in this cold layer (HDO/H_2O ∼ 5% and D_2O/HDO ∼ 11%). It seems, however, to decrease in the warm inner regions, as suggested by the upper limit of 0.9% derived for D_2O/HDO. The complete ice mantle sublimates at dust temperatures higher than 100 K (Fraser et al. 2001). The D/H ratios derived in these warm inner regions should then reflect the overall (gas + grain) deuteration of water. To constrain the water formation mechanisms in the inner protostellar region, it is, however, required to determine more precisely the D_2O/HDO ratio.

We report, in this Letter, the first detection of D_2O toward the Class 0 protostar NGC 1333 IRAS2A. This source is only the second low-mass protostar in which D_2O is detected. It is also the first interferometric observation of D_2O. The HDO $5_{4,2}$–$6_{3,3}$ transition at 317.2 GHz was also detected for the first time and is,

* Based on observations carried out with the IRAM Plateau de Bure Interferometer. IRAM is supported by INSU/CNRS (France), MPG (Germany) and IGN (Spain).

Table 1
Parameters from an Elliptical Gaussian Fit to the Continuum Emission

	IRAS2A
Synthesized beam	0.″89 × 0.″76 (+42°)
Flux (Jy)[a]	0.578 (±0.003)
R.A. (J2000)[a]	03:28:55.57 (±0.″002)
Decl. (J2000)[a]	31:14:37.07 (±0.″002)
Extent[b]	0.″95 × 0.″68 (+38°)

Notes.
[a] Errors given are the statistical errors from the fitting routine.
[b] Major × minor axis and position angle for elliptical Gaussian profile in the (u, v) plane.

to date, the most highly excited transition of HDO ($E_{up} = 691$ K) ever detected in a low-mass protostar. From these observations, we determine the D_2O/HDO ratio in the warm inner region of NGC 1333 IRAS2A, providing important constraints on water formation.

2. OBSERVATIONS

Observations of the low-mass protostar NGC 1333 IRAS2A were carried out with the IRAM Plateau de Bure Interferometer (PdBI) on 2013 December 3 in the C configuration under very good weather conditions. The para-D_2O $1_{1,0}$–$1_{0,1}$ transition was observed at 316.8 GHz using the narrow-band correlator with a spectral resolution of 0.078 MHz ($dv = 0.07$ km s^{-1}). The observations of the continuum emission and the HDO $5_{4,2}$–$6_{3,3}$ transition at 317.2 GHz have been obtained simultaneously using the WIDEX correlator that provides a spectral resolution of 1.95 MHz ($dv = 1.8$ km s^{-1} at 317.2 GHz). The data were calibrated and imaged using the CLIC and MAPPING packages of the GILDAS[8] software. Phase and amplitude were calibrated by observing the nearby strong quasars 0333+321 and 3C 84. The bandpass calibration was carried out on 3C 454.3, and the absolute flux density scale was derived from LkHα 101 and MWC 349. The continuum was subtracted before Fourier transformation of the line data.

The parameters of the continuum emission derived with an elliptical Gaussian fit to the (u, v) plane are presented in Table 1. The D_2O line is detected at the expected velocity of the source ($v_{LSR} = 7.0$ km s^{-1}). It is, however, blended with two other components at a velocity of ∼11.5 km s^{-1} and ∼15.0 km s^{-1} (see Figure 1). The first component is identified as the transition 7_0–6_0+ of CH_3OD ($\nu = 316.7951$ GHz; Anderson et al. 1993). The second component at 15 km s^{-1} corresponds to the CH_3OD 3_2–3_1+ transition ($\nu = 316.7916$ GHz), but the CH_3OCH_3 $22_{6,16}$–$22_{5,17}$ transitions ($\nu = 316.7908$, 316.7918, 316.7928 GHz) can also contribute to the line flux of this component. The presence of other species than D_2O around 7 km s^{-1} can be excluded using the spectroscopic databases. Although some CH_3CHO lines are detected in the WIDEX data, a local thermal equilibrium (LTE) modeling of these lines does not predict any emission for the $9_{1,8,8}$–$8_{1,8,7}$ transition ($\nu = 316.8034$ GHz) at a velocity of 7.9 km s^{-1}. The $SO^{17}O$ $11_{2,10}$–$10_{1,9}$ transition ($\nu = 316.7988$ GHz) cannot contribute to the line flux at 9.5 km s^{-1}, as the equivalent transition of the more abundant isotopologue $^{34}SO_2$ is not detected in the WIDEX data.

The total flux of the para-D_2O line was extracted with a three-Gaussian decomposition on each pixel where emission is detected, and is estimated to be 0.74 Jy km s^{-1}. The flux of the HDO line was measured in the (u, v) plane and is about 1.1 Jy km s^{-1}. A flux calibration uncertainty of 20% is assumed. The D_2O and HDO emission peaks are situated at the same position as the peak of the continuum emission (see Figure 1).

Three other HDO transitions were previously detected with the PdBI: the HDO $3_{1,2}$–$2_{2,1}$ and $2_{1,1}$–$2_{1,2}$ transitions at 225.9 and 241.6 GHz, respectively, by Persson et al. (2014) and the $4_{2,2}$–$4_{2,3}$ transition at 143.7 GHz by Taquet et al. (2013a). The $H_2^{18}O$ $3_{1,3}$–$2_{2,0}$ line was also detected at 203.4 GHz by Persson et al. (2012). The parameters of the different lines are summarized in Table 2. The different water isotopologues show full-width at half maximum (FWHM) of ∼4 km s^{-1}. The HDO lines at 317.2 and 143.7 GHz only show higher widths because of the lower spectral resolution of the WIDEX data.

3. RESULTS

Using the four HDO detections, we carried out a LTE analysis through the rotational diagram method (Goldsmith & Langer 1999). Because of the different beams of the observations, we considered beam dilution factors for different source sizes. We determined the best-fit through a χ^2 minimization. Good linear fits are obtained for source sizes smaller than 1″. The best agreement is found for a source size of 0.″5 (see Figure 2). It is relatively close to the extent (0.″4–0.″6) determined by a Gaussian fit in the (u, v) plane for the HDO lines at 225.9, 241.6 and 143.7 GHz. The column densities and excitation temperature derived are summarized in Table 3. For source sizes smaller than 0.″3, the optical thickness of the HDO lines at 225.9 and 241.6 GHz become non-negligible, and the four HDO line fluxes cannot be reproduced simultaneously anymore with a single excitation temperature. The similarity of the fitted line widths of the observed transitions is also favorable to their optical thinness or, at most, moderate optical thickness (see Table 2).

Using the flux derived from our D_2O observations and the same excitation temperature as HDO, we calculated the para-D_2O column density as a function of the source size (see Table 3). Assuming that the ortho/para(D_2O) ratio is 2:1 (LTE value at $T \gtrsim 20$ K), we determined a D_2O/HDO ratio of $(1.2 \pm 0.5) \times 10^{-2}$. We used the same procedure to estimate the para–$H_2^{18}O$ column density, using the flux of the transition $3_{1,3}$–$2_{2,0}$ detected by Persson et al. (2012). Assuming that the ortho/para ratio of $H_2^{18}O$ is 3:1, i.e., the equilibrium value at high temperature ($T > 50$ K), and that $H_2^{16}O/H_2^{18}O$ is 560 (Wilson 1999), the HDO/H_2O ratio is about $(1.7 \pm 0.8) \times 10^{-3}$. Neither the D_2O line nor the $H_2^{18}O$ line are optically thick for the considered source sizes.

As the upper energy level of the D_2O transition is lower (15 K) than those of the other lines (95–691 K), we also checked that a lower excitation temperature would not decrease considerably the D_2O/HDO ratio. To get a D_2O/HDO ratio as low as that of HDO/H_2O, the D_2O excitation temperature should be lowered to 30 K. This is excluded in the warm inner regions of protostars ($T > 100$ K) and could only occur if most of the D_2O emission arises from the cold outer envelope, which seems inconsistent with the observed spatial distribution.

With the non-LTE RADEX code (van der Tak et al. 2007), the fluxes of the HDO lines at 225.9, 241.6 and 143.7 GHz can only be reproduced when the H_2 density and the temperature are higher than 2×10^8 cm^{-3} and 125 K, respectively. The flux of the HDO line at 317.2 GHz cannot be estimated with this

[8] http://www.iram.fr/IRAMFR/GILDAS/

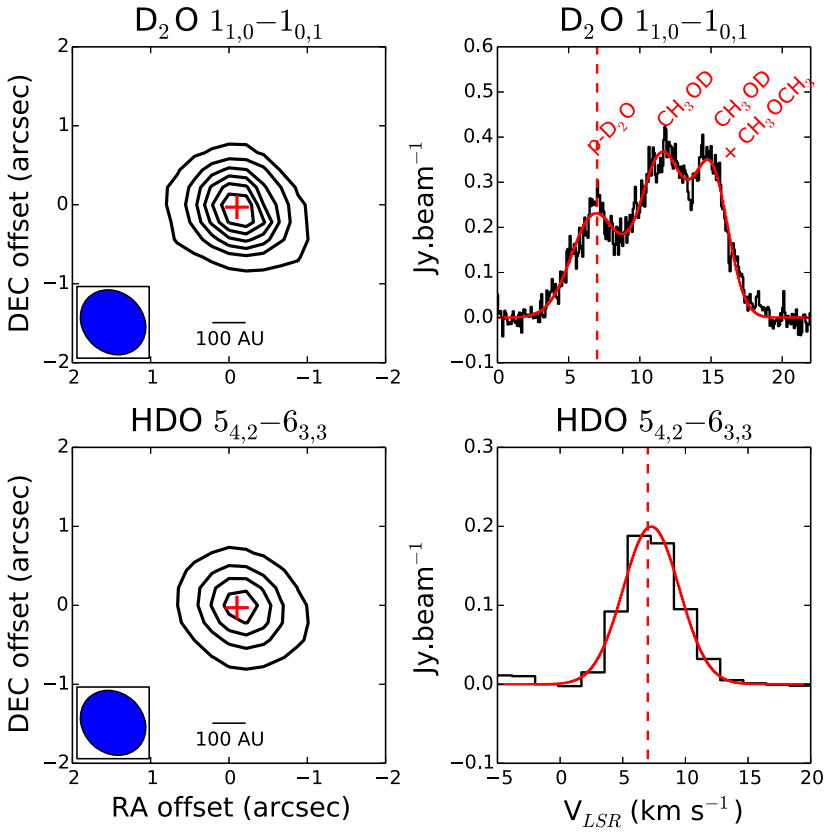

Figure 1. Left: integrated intensity maps for the para-D_2O $1_{1,0}$–$1_{0,1}$ and HDO $5_{4,2}$–$6_{3,3}$ lines. The reference position (0,0) is α_{2000}=03^{h}28^{m}55^s.58, δ_{2000}=+31°14′37″.1. The beam is shown in the lower left corner. The red cross shows the position of the peak of the continuum. Contours start at 50 mJy km s^{-1} (5σ) with steps of 150 mJy km s^{-1}. The integrated intensity map of D_2O is obtained using the three-Gaussian decomposition of the line profile. Right: continuum subtracted spectra of the para-D_2O $1_{1,0}$–$1_{0,1}$ and HDO $5_{4,2}$–$6_{3,3}$ lines (in black). The red line shows the results of the Gaussian fit.

(A color version of this figure is available in the online journal.)

Table 2
Parameters of the D_2O, HDO, and $H_2^{18}O$ Observed Lines[a]

Transition	Frequency (GHz)	E_{up} (K)	A_{ij} (s^{-1})	Beam (″ × ″)	Flux[b] (Jy km s^{-1})	Size[c] (″)	FWHM[d] (km s^{-1})	References[e]
p-D_2O $1_{1,0}$–$1_{0,1}$	316.7998	15	6.4×10^{-4}	0.9 × 0.8	0.74 ± 0.15	...[e]	3.8 ± 0.2	1
HDO $5_{4,2}$–$6_{3,3}$	317.1512	691	2.7×10^{-5}	0.9 × 0.8	1.10 ± 0.22	...[e]	5.3 ± 0.2	1
HDO $4_{2,2}$–$4_{2,3}$	143.7272	319	2.8×10^{-6}	2.2 × 1.8	0.67 ± 0.13	0.6 ± 0.2	6.7 ± 0.5	2
HDO $3_{1,2}$–$2_{2,1}$	225.8967	168	1.3×10^{-5}	1.3 × 1.0	3.98 ± 0.80	0.4 ± 0.1	4.1 ± 0.1	3
HDO $2_{1,1}$–$2_{1,2}$	241.5616	95	1.2×10^{-5}	1.2 × 0.9	3.88 ± 0.78	0.5 ± 0.1	4.0 ± 0.1	3
p-$H_2^{18}O$ $3_{1,3}$–$2_{2,0}$	203.4075	204	4.8×10^{-6}	0.9 × 0.7	0.98 ± 0.20	0.8 ± 0.1	4.0 ± 0.1	4

Notes.
[a] The HDO, D_2O, and $H_2^{18}O$ spectroscopic parameters come from the JPL and CDMS databases (Pickett et al. 1998; Müller et al. 2005).
[b] An observational uncertainty of 20% is assumed for each line. The data used in Taquet et al. (2013a) were reprocessed and the line flux re-measured.
[c] FWHM of the circular Gaussian fit in the (u, v) plane.
[d] FWHM measured toward the pixel showing the peak in emission. The higher FWHM for the HDO lines at 143.7 and 317.2 GHz are due to the lower spectral resolution of the WIDEX data (1.95 MHz).
[e] The (u, v) plane is best fitted by a point source.
References. (1) This study; (2) Taquet et al. (2013a); (3) Persson et al. (2014); (4) Persson et al. (2012).

method, as the collisional coefficients (with ortho and para-H_2) are only determined for the transitions with $E_{up} \leqslant 444$ K (Faure et al. 2012). The derived HDO and $H_2^{18}O$ column densities are similar to the LTE values presented earlier. The D_2O column density cannot, however, be determined with a non-LTE code, as the collisional coefficients available for D_2O (Faure et al. 2012) are only calculated with para-H_2 for the first six energy levels ($E_{up} < 112$ K). They are thus not suited for estimates in warm regions ($T \gtrsim 100$ K).

4. DISCUSSION

4.1. High D_2O/HDO Ratio versus Low HDO/H_2O Ratio

Statistically, the replacement of a H atom by a D atom would lead to a D_2O/HDO ratio four times lower than the HDO/H_2O ratio. Surprisingly, we derived, in the inner region of NGC 1333 IRAS2A, a D_2O/HDO ratio a factor seven higher than the HDO/H_2O ratio. Even considering the estimated

Table 3
Water Deuterium Fractionation Derived with the LTE Analysis[a]

Source Size (″)	N(HDO) ($\times 10^{17}$ cm^{-2})	T_{ex} (K)	χ^2	N(p–D_2O) ($\times 10^{14}$ cm^{-2})	N(p–$H_2^{18}O$) ($\times 10^{16}$ cm^{-2})	D_2O/HDO ($\times 10^{-2}$)	HDO/H_2O ($\times 10^{-3}$)	D_2O/H_2O ($\times 10^{-5}$)
0.3	2.5 ± 0.9	212 ± 20	0.45	9.4 ± 2.0	6.1 ± 1.6	1.1 ± 0.5	1.8 ± 0.8	2.0 ± 0.7
0.4	1.5 ± 0.5	215 ± 20	0.28	5.9 ± 1.2	3.8 ± 1.1	1.2 ± 0.5	1.8 ± 0.8	2.1 ± 0.7
0.5*	1.0 ± 0.4	218 ± 21	0.19	4.2 ± 1.0	2.7 ± 0.8	1.2 ± 0.5	1.7 ± 0.8	2.1 ± 0.8
0.6	0.8 ± 0.3	221 ± 21	0.23	3.4 ± 0.8	2.2 ± 0.6	1.3 ± 0.6	1.6 ± 0.8	2.1 ± 0.8
0.7	0.6 ± 0.2	224 ± 22	0.44	2.9 ± 0.7	1.8 ± 0.5	1.4 ± 0.6	1.5 ± 0.7	2.1 ± 0.8
0.8	0.5 ± 0.2	227 ± 23	0.80	2.6 ± 0.5	1.6 ± 0.4	1.5 ± 0.6	1.4 ± 0.6	2.2 ± 0.7

Notes.
[a] We assumed a flux calibration uncertainty of 20% for each line. The uncertainty on the D_2O and $H_2^{18}O$ column densities include both the flux calibration uncertainty and the excitation temperature uncertainty. For the determination of the ratios, we assumed ortho/para(D_2O) = 2, ortho/para($H_2^{18}O$) = 3, and $H_2^{16}O/H_2^{18}O = 560$.
* Best-fit obtained with the χ^2 minimization.

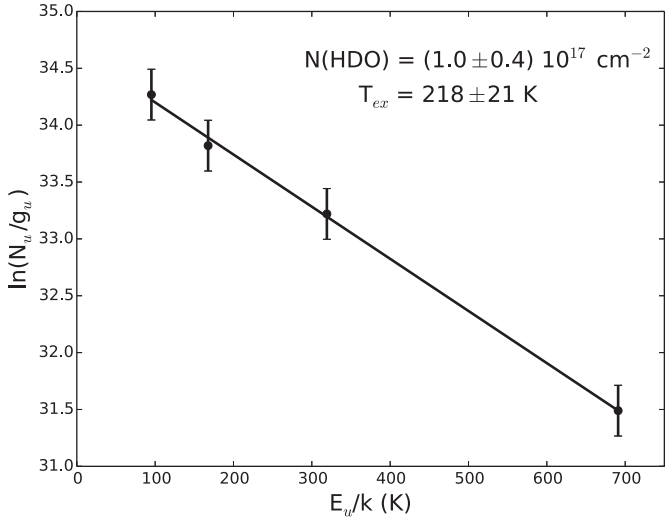

Figure 2. Rotational diagram of HDO for a source size of 0.″5.

uncertainties from the analysis (see Table 3), a significant difference is observed between these ratios.

A lower D_2O/HDO ratio could be obtained if the ortho/para ratio of D_2O were below the LTE value of 2. Indeed, a value of ∼1.1–1.3 was derived in the cold absorbing layer of IRAS 16293−2422 (Vastel et al. 2010; Coutens et al. 2013a). For an ortho/para ratio equal to 1, the D_2O/HDO ratio would be about 9×10^{-3}. The mechanisms leading to an ortho/para ratio of D_2O lower than 2 are, however, not understood. There is therefore no evidence that the ortho/para ratio in the warm gas would be the same as in the cold gas.

The HDO/H_2O ratio of $(1.7 \pm 0.8) \times 10^{-3}$ derived here is a factor of two higher than the LTE estimate without beam dilution by Persson et al. (2014) and a factor of two lower than the non-LTE estimate by Taquet et al. (2013a) for a H_2 density of 10^8 cm^{-3}. Persson et al. (2014) obtain a higher HDO/H_2O ratio of ∼(2–3) × 10^{-3} with a non-LTE excitation and radiative transfer model using a spherical envelope model with a temperature and density gradient constrained from other observations. Even considering HDO/H_2O ratios of ∼(2–3) × 10^{-3} derived in these two studies, our observed D_2O/HDO ratio is still a factor 4–6 higher.

The highest difference of a factor of seven between the HDO/H_2O and D_2O/HDO ratios is found for the inner regions of NGC 1333 IRAS2A. In contrast, the D_2O/HDO ratio is only a factor of two higher than HDO/H_2O for the cold absorbing layer of IRAS16293−2422 (Coutens et al. 2012, 2013a), while it is a factor of two lower for the hot core of Orion KL (D_2O/HDO ∼ 1.6 × 10^{-3} versus HDO/H_2O∼3 × 10^{-3}; Neill et al. 2013).

Water observed in low-mass sources is formed mostly on the grains and then thermally desorbed in the warm inner regions of protostars ($T_d \gtrsim 100$ K). The gas-phase water D/H ratios then reflect the water deuterium fractionation in the icy grain mantles formed earlier in the molecular cloud and/or prestellar core by hydrogenation (and deuteration) of atomic or molecular oxygen. In the earliest molecular cloud phase, the deuterium fractionation is less than in the cold and dense prestellar stage, so the ice mantles are expected to have a layered structure, with the highest deuteration fractions on top (Taquet et al. 2014). In the outer regions, these top ice layers are photodesorbed resulting in high gas-phase HDO and D_2O abundances. In the inner envelope, the entire ice mantle thermally desorbs and the gas-phase abundances reflect the lower, less deuterated ice layers.

Quantitative predictions of the D_2O/HDO and HDO/H_2O ratios have been obtained with pseudo-time dependent chemical models in which the physical conditions are constant (Taquet et al. 2013b; Albertsson et al. 2013) and with 1D dynamical models in which a parcel of gas experiences different physical conditions with time (Cazaux et al. 2011; Coutens et al. 2013a; Aikawa et al. 2012; Taquet et al. 2014; Wakelam et al. 2014). In the pseudo-time-dependent models, the water observed in the inner region comes from the sublimation of the ice mantles and can subsequently evolve chemically by gas-phase reactions, while in the dynamical models, the molecules remain in the warm gas for such a short time due to the rapid infall that no further chemistry can take place. None of these models predict D_2O/HDO ratios higher than HDO/H_2O ratios, contrary to what is observed in NGC 1333 IRAS2A.

This discrepancy between models and observations could mean that the water deuteration on grain surfaces is far from understood and that some deuteration pathways are incorrect or missing in the different chemical models. A second explanation could be that, in addition to the thermal desorption, water is also formed at high temperature (≳230 K) through the following reactions:

$$O + H_2 \rightarrow OH + H, \quad (1)$$

$$OH + H_2 \rightarrow H_2O + H. \quad (2)$$

These gas-phase reactions do not play a major role in the pseudo-time dependent models by Taquet et al. (2013b) and Albertsson et al. (2013), as the temperatures considered were

lower than 150 K. The thermal desorption of grain mantles would then result in the production of high D_2O/HDO ratios that reflect the water formation at low temperatures on grain surfaces, while the gas-phase reactions at high temperature would produce a lot of H_2O and little deuterated water, resulting in a low HDO/H_2O ratio. In this interpretation, the D_2O/HDO ratio determined in NGC 1333 IRAS2A ($\sim$1.2%) would reflect the ratio present in the ices. This value is in agreement with the predictions of a chemical model including the multilayer ice mantle approach and coupled with a 1D dynamical model, where $\sim(0.5\text{–}3) \times 10^{-2}$ is found in the inner regions of a typical Class 0 protostar (Taquet et al. 2014). It is also similar to the upper limit constrained in the inner regions of IRAS 16293−2422 (Coutens et al. 2013a; $\leqslant$0.9%).

The high temperature gas-phase reactions (1) and (2) can take place both in the quiescent inner regions of protostellar envelopes where the temperature is above 230 K and in shocks. An extended component of $H_2^{18}O$ attributed to outflows was detected toward NGC 1333 IRAS2A (Persson et al. 2012). The base of the jet at the position of the protostar could possibly contribute to the $H_2^{18}O$ flux. There is, however, no spectral evidence of that. The line profile of the $H_2^{18}O$ line is narrow and similar to those of deuterated water. Besides, Persson et al. (2014) show that the HDO/H_2O ratios derived in NGC 1333 IRAS2A are similar to NGC 1333 IRAS4A and IRAS4B, but no extended emission of $H_2^{18}O$ along outflows is detected toward these two sources. If these sources do not show outflow emission, their HDO/H_2O ratio should be higher, unless they present lower D_2O/HDO ratios than in NGC 1333 IRAS2A. H_2O could also be produced by accretion shocks when material falls onto the disk (Neufeld & Hollenbach 1994), but as previously noted, the different water isotopologues show similar and relatively narrow line widths, which does not favor a shock scenario. Water formation in accretion shocks was also rejected for the low-mass protostar NGC 1333 IRAS4B (Jørgensen & van Dishoeck 2010). Consequently, if water is formed by gas-phase reactions at high temperature in low-mass protostars, it would probably take place in quiescent regions, rather than in shocks.

These results highlight the importance of further experimental and theoretical studies of gas and grain surface deuteration. Dynamical effects can also be crucial for the chemistry. In two-dimensional dynamical models including rotation and possibly disk formation, the time that the thermally desorbed molecules spend in the warm gas is lengthened considerably (e.g., Visser et al. 2009) so that warm gas-phase chemistry becomes important in addition to the grain surface chemistry. Such models should be attempted to check that the HDO/H_2O and D_2O/HDO ratios found in NGC 1333 IRAS2A can be reproduced. Very high spatial resolution observations at 0.″1 scale may be able to distinguish the various scenarios and fully rule out a shock contribution. If $H_2^{18}O$ shows enhanced emission in the innermost and warmest regions (within $\sim$30 AU), while HDO and D_2O do not, it would favor gas-phase formation of water at high temperatures. On the contrary, if the different isotopologues show a similar distribution, it would imply a missing ingredient in our understanding of the surface deuteration process.

4.2. The D_2O/HDO Ratio from the Cold Outer to the Warm Inner Regions

No measurement of the D_2O/HDO ratio has been obtained in the cold absorbing layer of NGC 1333 IRAS2A. If we assume that it is similar to the D_2O/HDO ratio measured in the cold layer surrounding IRAS 16293−2422 ($\sim$11%) or to the HDO/H_2O ratio derived in the cold envelope of NGC 1333 IRAS2A by Liu et al. (2011, $\sim$7%), this would imply that the D_2O/HDO ratio decreases by a factor 6–10 from the cold to the warm regions. This is consistent with the variations of the D_2O/HDO ratio measured in IRAS 16293−2422 (Coutens et al. 2013a).

Such a decrease in the water deuterium fractionation from the cold to the warm gas can be explained by the differential deuteration of the multilayer ice mantles at the range of densities and temperatures encountered prior to and during the star formation process (Taquet et al. 2014). If disks are present in the inner regions at the Class 0 stage, turbulent mixing could also explain some decrease of the water D/H ratio (Furuya et al. 2013; Albertsson et al. 2014) but this would require a significant fraction of the emission to arise from the disk rather than envelope.

The authors thank the IRAM staff and especially Tessel van der Laan for their help with the observations and reduction of the data.

REFERENCES

Aikawa, Y., Wakelam, V., Hersant, F., Garrod, R. T., & Herbst, E. 2012, ApJ, 760, 40
Albertsson, T., Semenov, D., & Henning, T. 2014, ApJ, 784, 39
Albertsson, T., Semenov, D. A., Vasyunin, A. I., Henning, T., & Herbst, E. 2013, ApJS, 207, 27
Anderson, T., Herbst, E., & Delucia, F. C. 1993, JMoSp, 159, 410
Butner, H. M., Charnley, S. B., Ceccarelli, C., et al. 2007, ApJL, 659, L137
Cazaux, S., Caselli, P., & Spaans, M. 2011, ApJL, 741, L34
Ceccarelli, C., Caselli, P., Bockelee-Morvan, D., et al. 2014, Protostars & Planets VI, ed. H. Beuther et al., in press (arXiv:1403.7143)
Codella, C., Ceccarelli, C., Nisini, B., et al. 2010, A&A, 522, L1
Coutens, A., Vastel, C., Caux, E., et al. 2012, A&A, 539, A132
Coutens, A., Vastel, C., Cazaux, S., et al. 2013a, A&A, 553, A75
Coutens, A., Vastel, C., Cabrit, S., et al. 2013b, A&A, 560, A39
Faure, A., Wiesenfeld, L., Scribano, Y., & Ceccarelli, C. 2012, MNRAS, 420, 699
Fraser, H. J., Collings, M. P., McCoustra, M. R. S., & Williams, D. A. 2001, MNRAS, 327, 1165
Furuya, K., Aikawa, Y., Nomura, H., Hersant, F., & Wakelam, V. 2013, ApJ, 779, 11
Goldsmith, P. F., & Langer, W. D. 1999, ApJ, 517, 209
Hartogh, P., Lis, D. C., Bockelée-Morvan, D., et al. 2011, Natur, 478, 218
Jørgensen, J. K., & van Dishoeck, E. F. 2010, ApJL, 710, L72
Liu, F.-C., Parise, B., Kristensen, L., et al. 2011, A&A, 527, A19
Müller, H. S. P., Schlöder, F., Stutzki, J., & Winnewisser, G. 2005, JMoSt, 742, 215
Neill, J. L., Wang, S., Bergin, E. A., et al. 2013, ApJ, 770, 142
Neufeld, D. A., & Hollenbach, D. J. 1994, ApJ, 428, 170
Parise, B., Caux, E., Castets, A., et al. 2005, A&A, 431, 547
Persson, M. V., Jørgensen, J. K., & van Dishoeck, E. F. 2012, A&A, 541, A39
Persson, M. V., Jørgensen, J. K., & van Dishoeck, E. F. 2013, A&A, 549, L3
Persson, M. V., Jørgensen, J. K., van Dishoeck, E. F., & Harsono, D. 2014, A&A, 563, A74
Pickett, H. M., Poynter, R. L., Cohen, E. A., et al. 1998, JQSRT, 60, 883
Raymond, S. N., Quinn, T., & Lunine, J. I. 2004, Icar, 168, 1
Stark, R., Sandell, G., Beck, S. C., et al. 2004, ApJ, 608, 341
Taquet, V., Charnley, S. B., & Sipilä, O. 2014, ApJ, 791, 1
Taquet, V., López-Sepulcre, A., Ceccarelli, C., et al. 2013a, ApJL, 768, L29
Taquet, V., Peters, P. S., Kahane, C., et al. 2013b, A&A, 550, A127
van der Tak, F. F. S., Black, J. H., Schöier, F. L., Jansen, D. J., & van Dishoeck, E. F. 2007, A&A, 468, 627
van Dishoeck, E. F., Herbst, E., & Neufeld, D. A. 2013, ChRv, 113, 9043
Vastel, C., Ceccarelli, C., Caux, E., et al. 2010, A&A, 521, L31
Visser, R., van Dishoeck, E. F., Doty, S. D., & Dullemond, C. P. 2009, A&A, 495, 881
Wakelam, V., Vastel, C., Aikawa, Y., et al. 2014, MNRAS, submitted
Wilson, T. L. 1999, RPPh, 62, 143